

<https://doi.org/10.1038/s41612-024-00633-1>

# Long range transport of South and East Asian anthropogenic aerosols counteracting Arctic warming

Check for updates

Suvarna Fadnavis<sup>1</sup> ✉, Sunil M. Sonbawne<sup>1</sup>, Anton Laakso<sup>2</sup>, Felix Ploeger<sup>3</sup>, Alexandru Rap<sup>4</sup>, Bernd Heinold<sup>5</sup>, T. P. Sabin<sup>1</sup> & Rolf Müller<sup>3</sup>

The large-scale convection during the Asian summer monsoon plays an important role in the rapid transport of boundary layer aerosols into the Asian summer monsoon anticyclone. Here, using the state-of-the-art ECHAM6–HAMMOZ aerosol-chemistry-climate model, we show that these aerosols are further transported to the Arctic along isentropic surfaces by the Brewer-Dobson-Circulation (BDC) during the monsoon season. Our model simulations show that East and South Asian anthropogenic emissions contribute significantly to the aerosol transported to the Arctic, which causes a higher negative net aerosol radiative forcing at the surface (dimming) of  $-0.09 \pm 0.02 \text{ Wm}^{-2}$  and  $-0.07 \pm 0.02 \text{ Wm}^{-2}$ , respectively. Over the Arctic, the East Asian anthropogenic aerosols that include large amounts of sulfate cause a seasonal mean net radiative forcing at the top of the atmosphere (TOA) of  $-0.003 \pm 0.001 \text{ Wm}^{-2}$  and a surface cooling of  $-0.56 \text{ K}$  while the black carbon dominated aerosol from South Asia shows a positive TOA forcing of  $+0.004 \pm 0.001 \text{ Wm}^{-2}$  with an only minor surface cooling of  $-0.043 \text{ K}$ . Overall, the long-range transport of South Asian aerosols results in a notably warming throughout the atmospheric column but minimal temperature response at the Arctic surface. Conversely, East Asian aerosols cool the troposphere and heat the lower stratosphere in the Arctic. The Asian aerosol thus plays an ambivalent role, with the East Asian sources in particular having the potential to counteract the rapid rise in Arctic temperatures and the associated melting of snow and ice.

The Arctic region is highly vulnerable to climate change<sup>1</sup>. The land surface temperature is increasing at a rate of  $0.5 \text{ }^\circ\text{C}$  per decade since the late 1970s, which is more than the global temperature increase<sup>2,3</sup>. This phenomenon is thus referred to as Arctic amplification<sup>4</sup>. The impacts of Arctic amplification manifest across various facets including extremes, ecosystems, marine biology, soils and permafrost, Arctic ice sheets, glaciers, society, and humans over Arctic<sup>5</sup>. Moreover, these effects extend to regions south of the Arctic, resulting in rising sea levels, shifting temperature and precipitation patterns, and heightened frequency of severe weather events<sup>6</sup>.

While Arctic amplification is driven by increases in anthropogenic greenhouse gases (GHG) and involved feedback mechanisms<sup>4</sup>. The short-lived climate forcing component, such as aerosol, are also important drivers of Arctic climate<sup>4</sup>. The enhanced amounts of black carbon (BC) aerosols in

the Arctic are of particularly concern because of its positive climate forcing (heating effect)<sup>7,8</sup> to amplify the warming effect caused by GHG. Another effect of BC aerosols is snow darkening due to the deposition of particles, hence reducing the surface albedo<sup>9,10</sup>. The darkened snow absorbs the radiation leading to surface warming, resulting in a modification in seasonal snow melting and aging, sea ice thinning, and glacier melting<sup>11</sup>. Thus, BC aerosol in particular is contributing to the current warming of the Arctic, which is estimated to be ice-free by the summer of 2050<sup>12</sup>. On the other hand, the climate warming by BC aerosol is offset by the cooling effect by sulfate aerosols<sup>13</sup>. A 20% global reduction in anthropogenic  $\text{SO}_2$  emissions would therefore lead to a positive net (solar and thermal) direct radiative forcing (aerosol-radiation interactions [RFari]) at the top of the atmosphere (TOA) of  $+0.019 \text{ Wm}^{-2}$  in the Arctic<sup>14</sup>.

<sup>1</sup>Indian Institute of Tropical Meteorology, Centre for Climate Change Research, MoES, Pune, India. <sup>2</sup>Finnish Meteorological Institute, Kuopio, Finland. <sup>3</sup>Forschungszentrum Jülich GmbH, IEK-7 Jülich, Germany. <sup>4</sup>School of Earth and Environment, University of Leeds, Leeds, UK. <sup>5</sup>Leibniz Institute for Tropospheric Research (TROPOS), Jülich, Germany. ✉e-mail: [suvarna@tropmet.res.in](mailto:suvarna@tropmet.res.in)

Past studies show that large amounts of carbonaceous (BC and organic aerosols) and sulfate aerosols are transported to the Arctic from different source regions. According to multi-model simulations for the year 2001<sup>15</sup>, reducing anthropogenic emissions by 20% resulted in decreased black carbon (BC) levels in the Arctic from sources in Europe (ranging from 21% to 74%), East Asia (ranging from 16% to 47%), and South Asia (ranging from 2% to 17%). These simulations also show decrease in sulfate aerosol levels in the Arctic between 31% and 71% from European sources, between 13% and 41% from East Asian sources, and between 1% and 7% from South Asian sources. Simulations of the Community Atmosphere Model, equipped with Explicit Aerosol Source Tagging show that concentrations of sulfate and BC in the Arctic has increased from sources in South and East Asia. Such increase has led to positive trends in these aerosols at the upper troposphere in the Arctic<sup>13</sup>.

The climate impact caused by aerosol-radiation interactions is determined by the extent to which aerosol can scatter and absorb solar radiation. For sulfate aerosols the overall effect is a cooling, due to their efficient scattering properties<sup>15</sup>, while for BC their absorption properties have been shown to lead to an overall warming effect<sup>7</sup>. Existing studies show that global sulfur emission caused a cooling rate of  $-0.020$  to  $-0.025$  K (TgS)<sup>-1</sup> yr<sup>-1</sup> in the Arctic and that BC emissions warm the atmosphere<sup>16</sup> leading to an increase in Arctic surface air temperature ( $+0.40$  K) during the 20th century<sup>17</sup>. BC emissions from Europe and North America caused a higher increase in Arctic surface air temperature by  $0.06$ – $0.1$  K Tg<sup>-1</sup> BC yr<sup>-1</sup> than Asian emissions ( $0.05$ – $0.08$  K Tg<sup>-1</sup> BC yr<sup>-1</sup>)<sup>18,19</sup>. Model simulations suggest that European emissions dominate the Arctic near-surface aerosol loading, but emissions from South and East Asia dominate the upper troposphere aerosol amounts<sup>20</sup>. The simulation using the source-tagging technique showed that the long-range transport from East Asia and South Asia maximizes at 9–12 km<sup>14</sup>. Global model simulations further show the transport of aerosols emitted from South Asia to the Arctic through the upper troposphere and lower stratosphere (UTLS)<sup>21</sup>. Long-range transport of aerosols from East Asia to the Arctic in the upper troposphere is also evident in CALIPSO observations<sup>22</sup>. The observations during the Arctic Research of the Composition of the Troposphere from Aircraft and Satellites (ARCTAS) campaign along with a chemical transport model also showed the transport of BC from the Asian continent to the Arctic via UTLS<sup>23</sup>. The transport of the majority of East Asian aerosol occurs near 3–6 km and partly through the upper troposphere near 8–10 km during convective events<sup>22,24</sup>. There may be rapid transport of East Asian dust to the Arctic within 5 days through the mid-troposphere (850–500 hPa)<sup>25</sup>. Lagrangian trajectory models show BC aerosols from South Asia travel over Central Asia and to the Arctic in 7 days<sup>26</sup>. However, East Asia contributes substantially more to the BC at higher altitudes<sup>27,28</sup>.

In this paper, we explore the transport of aerosols emitted from South and East Asia to the Arctic during the monsoon season, since the monsoon convection is known to play an important role in the efficient transport of aerosols and their precursors to the UTLS<sup>29–32</sup>. During the summer season, the Asian UTLS region is featured with a large-scale anticyclonic circulation system containing the maximum amount of aerosols and trace gases as evident in satellite retrievals and in-situ measurements<sup>32–36</sup>. The monsoon anticyclone is associated with an aerosol layer, the Asian Tropopause Aerosol Layer (ATAL), whose composition is a subject of research till date. The previous studies report presence of BC, OC, nitrates and sulfate aerosols in the ATAL<sup>21,29,37</sup>. Recent StratoClim (Stratospheric and upper tropospheric processes for better climate predictions) Aircraft measurements in the monsoon in 2017 showed this later mainly consists of ammonium nitrate (AN) and organics<sup>38,39</sup>. In this paper, we analyze anthropogenic aerosols BC, OC and sulfate in the anticyclone and their transport to the Arctic. Previous model simulations have indicated the presence of two transport branches supplying aerosols to the UTLS from (1) South Asia and (2) East Asia<sup>40</sup>. These aerosols and trace gases in the South and East Asian UTLS may get transported further to the Arctic. While existing studies show evidence of transport from East Asia to the Arctic through the UTLS<sup>41</sup>, the detailed transport pathways of South and

East Asian aerosols to the Arctic during the monsoon season have not yet been fully investigated.

Here, using three sets of the state-of-art ECHAM6–HAMMOZ chemistry-climate model simulations (1) control simulation (CTL) includes all emissions, sensitivity simulations for (2) South Asian anthropogenic aerosols switched off (SAS0), and, (3) East Asian anthropogenic aerosols switched off (EAS0), we show the pivotal role of large-scale Asian summer monsoon convection in facilitating the efficient transport of boundary layer aerosols from South and East Asia to the UTLS. From there, propelled by the Brewer-Dobson Circulation (BDC), these aerosols journey to the Arctic region. Additionally, our sensitivity simulations shed light on impacts of South Asian versus East Asian aerosols on the Arctic environment.

## Results and discussion

### Transport of South Asian and East Asian aerosols into the monsoon anticyclone and the Arctic region

During the Boreal summer, the Asian summer monsoon is the most extensive dynamical system in the Northern Hemisphere, consisting of convergent cyclonic flow in the lower troposphere and strong divergent anticyclonic flow in the UTLS<sup>32</sup>. The Asian summer monsoon anticyclone (ASMA) stretches from western Africa to the western Pacific Ocean (30°–130° E, 15°–45° N)<sup>29,42</sup>. The deep monsoon convection plays an important role in the efficient transport of surface pollutants from Asia (aerosols and gases) into the UTLS as evident both in satellite data<sup>32,43</sup> and in-situ measurements<sup>34,35,44</sup>. In the ASMA UTLS region maximum aerosol concentrations are seen near 14–18 km in CALIPSO scattering ratio and balloon-sonde observations<sup>35,40</sup>.

Within the Asian region, aerosol emission hot spots are located over North India and East China (Supplementary Fig. 1). These aerosols are partly lifted to the monsoon anticyclone via convection over (1) the Bay of Bengal and the Southern slopes of the Himalayas (i.e. South Asian transport branch) and (2) the South China Sea and Western Pacific (i.e. East Asian transport branch)<sup>40</sup>. We analysed the contribution of South Asian versus East Asian aerosols reaching the UTLS and their transport to the Arctic on isentropic levels. This approach is chosen because long-range transport is more accurately depicted on surfaces of constant potential temperature<sup>45</sup>.

Figure 1 shows the distribution of anomalies for anthropogenic BC, OC, and sulfate aerosols for South Asian aerosols (CTL - SAS0) and East Asian aerosols (CTL - EAS0) in the monsoon anticyclone region at the  $\sim 380$  K potential temperature level. Figure 1a–d shows that the amounts of anomalies of aerosols in the monsoon anticyclone are larger for South Asia (68°E–95°E, 8°N–38°N) than for East Asia (78°E–145°E, 20°N–50°N) by  $1.2$  ng m<sup>-3</sup> of BC,  $3$  ng m<sup>-3</sup> of OC, and  $20$  ng m<sup>-3</sup> of sulfate. Interestingly, the sulfate aerosol distribution shows a high amount in the Arctic for East Asian emissions in comparison to South Asian emissions by  $50$  ng m<sup>-3</sup>. At the Arctic, near 380 K potential temperature level, a large amount of East Asian aerosols is due to the accumulation of sulfate and partially due to their vertical transport from the lower levels by the monsoon convection. Figure 1 also shows that the South and East Asian aerosols injected into the monsoon anticyclone are further transported to the western Pacific by westerly winds. In addition, the vertical extent of heat-driven convection at the southern slopes of the Himalayas seems to extend to higher altitudes than in East Asia which plays an important role in lifting South Asian aerosols deep into the UTLS. Negative anomalies of sulfate aerosols in Fig. 1e are due to the oxidation of SO<sub>2</sub> by OH that produced H<sub>2</sub>SO<sub>4</sub> which is less in the CTL simulation compared to the SAS0 simulation at 380 K potential temperature level (see Supplementary Fig. 2).

Our model simulations show that the East Asian aerosols show larger outflow over the Western Pacific than South Asian aerosols. These East Asian aerosols are then transported northward to the Arctic. The higher amounts of East Asian sulfate aerosols at the Arctic seen in Fig. 1f is mostly due to the transport from the lower level by monsoon convection and its accumulation. In fact, aerosols emitted from East and South Asia (BC, OC and sulfate) are also transported to the Southern hemisphere ( $\sim 40^\circ$ S) through westerly ducts in the upper troposphere from the Northern extra-tropics to the southern

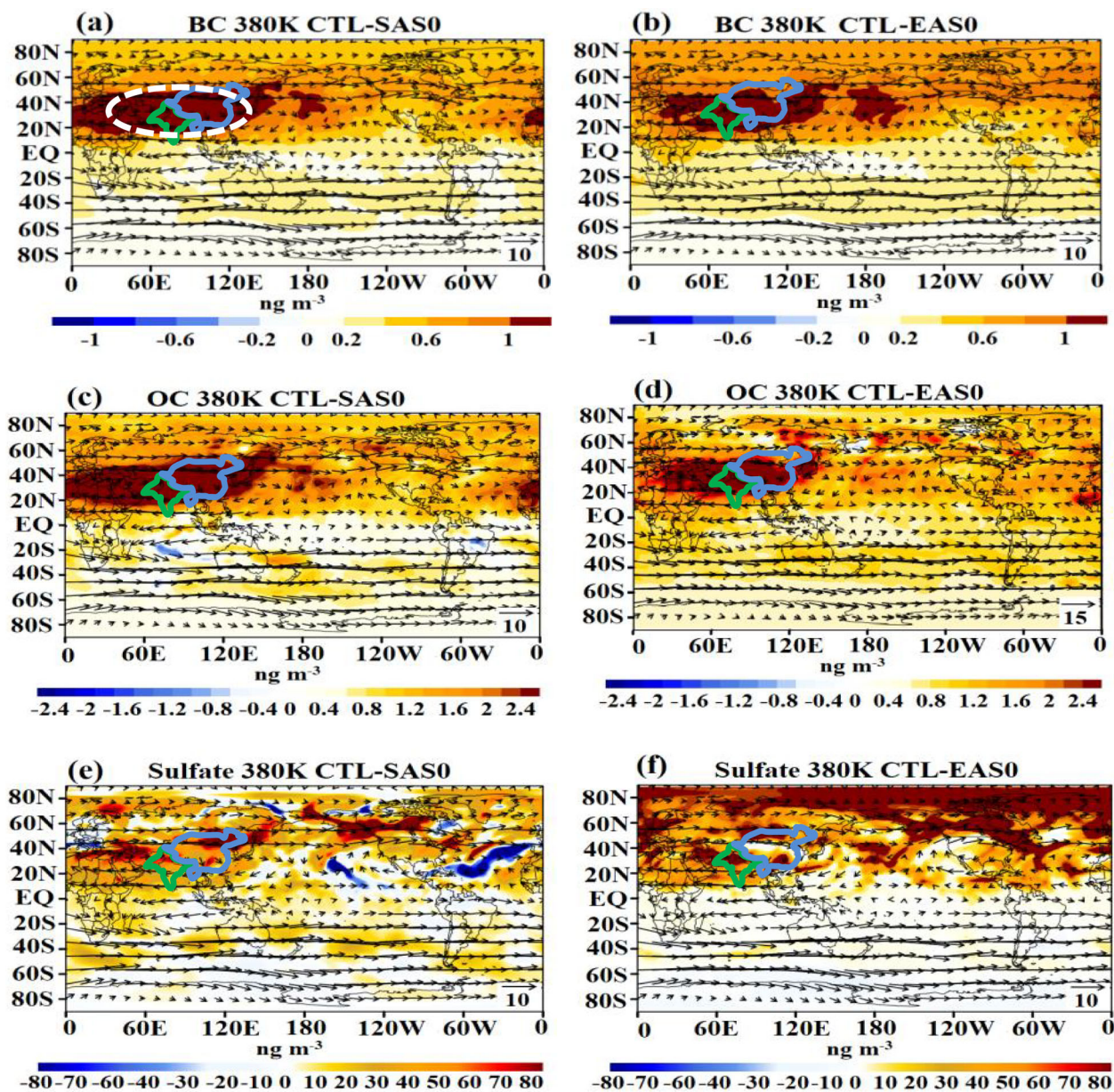


**Fig. 1 | Distribution of anthropogenic aerosols in the Asian summer monsoon anticyclone.** The spatial distribution of anomalies of BC ( $\text{ng m}^{-3}$ ) at 380 K potential temperature level for a South Asian (CTL - SASO), b and East Asian (CTL - EASO), c, d same as (a, b) but for OC, e, f same as (a, b) but for sulfate aerosols. Wind vectors are plotted from CTL simulations. The boundaries of South Asia (Green) and East

Asia (Blue) considered in this study are indicated in (a–h). The region of Asian summer monsoon anticyclone ( $30^{\circ}$ – $130^{\circ}\text{E}$ ,  $15^{\circ}$ – $45^{\circ}\text{N}$ ) is indicated in white dashed line in (a). (Figure created using the COLA/GrADS software).

extra-tropics<sup>46</sup>. However, this southward transport is weak for East Asian sulfate aerosols.

The simulated transport of aerosols to the Arctic is in agreement with observations. Aircraft campaign data from North American Arctic region show that Asian BC was transported in the upper troposphere ( $5 \text{ ng m}^{-3}$ ) over the North American Arctic in summer<sup>23</sup>. The transport of BC aerosols from the Indo-Gangetic plain in South Asia to the Arctic occurs within 7 days in the upper troposphere in summer season<sup>26</sup>. Past studies<sup>22</sup> reported that in summer transports tracers released over Asia into the Arctic occurs in 9–20 days.

We analyse the transport of South and East Asian aerosols from the ASMA to the Arctic ( $0^{\circ}$ – $360^{\circ}$ ,  $65^{\circ}$ – $90^{\circ}\text{N}$ ). Figure 2 shows the vertical distribution of BC, OC, and sulfate aerosols averaged over the ASAM region ( $30^{\circ}$ – $130^{\circ}\text{E}$ )<sup>21,29,47–49</sup>. The satellite retrievals and aircraft measurements show the maximum concentration of aerosols and gases in the eastern ASMA

region<sup>31–33,44,50</sup>. The convection, indicated by the distribution of cloud droplet number concentration along with ice crystal number concentrations and wind vectors in Fig. 2g, shows that the monsoon convection lifts the aerosols from the boundary layer of South Asia and East Asia to the anticyclone from where they are further transported to the Arctic via the UTLS (340–420 K). The convection indicated over South Asia ( $70^{\circ}\text{E}$ – $90^{\circ}\text{E}$ ) extends to a higher altitude ( $\sim 360 \text{ K}$  potential temperature level) than over East Asia ( $340 \text{ K}$  potential temperature level) (CDNC + ICNC:  $5 \text{ mg}^{-1}$ ) (Fig. 2g), likely influenced by the high elevation of the Himalayas. The distribution of CDNC and ICNC and vertical velocity plot at 350 K potential temperature level also indicates higher convection over the South Asia (Tibetan Plateau region) than East Asia (Fig. 2h). As a consequence, the outflow of South Asian aerosol occurs at higher levels than for East Asian aerosols. The South Asian and East Asian aerosols entrain the shallow branch of the Brewer Dobson circulation (BDC), driven by the EP flux convergence<sup>51</sup>.

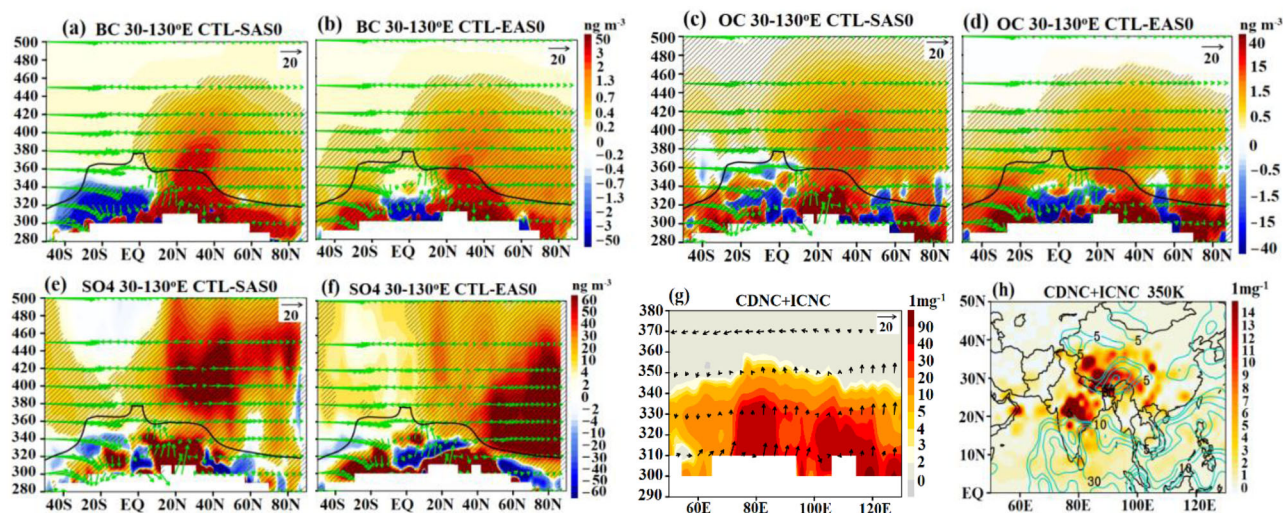


**Fig. 2 | Vertical transport of aerosols from South Asia and East Asia and role of monsoon convection.** Latitude potential temperature section of anomalies of BC aerosols ( $\text{ng m}^{-3}$ ) for South Asia (CTL-SASO) and East Asia (CTL-EASO)

**a, b** averaged for Asian summer monsoon anticyclone ( $30^{\circ}$ – $130^{\circ}$  E), **c, d** same as (**a, b**) but for OC aerosols, **e–h** same as (**a–d**) but for sulfate aerosols, the black contour of 2 PV (Potential vorticity PV,  $1\text{PVU} = \text{m}^2 \text{K kg}^{-1} \text{s}^{-1} 10^{-6}$ ) in (**a–f**) indicates the dynamical tropopause, the dynamical tropopause is identified as 2 PVU and

380 K in the tropics, **g** vertical distribution of cloud droplet number concentration along with ice crystal number concentration ( $\text{m g}^{-1}$ ) averaged for  $10^{\circ}$ – $30^{\circ}$ N and the monsoon season. Wind vectors are indicated in green color in (**a–f**) and black in (**g, h**) spatial distribution of cloud droplet number concentration along with ice crystal number concentration ( $\text{m g}^{-1}$ ) at 350 K potential temperature level (in shades) and contours in cyan indicate vertical velocity field ( $\text{m s}^{-1}$ ). The vertical velocity field is scaled by 300. (Figure created using the COLA/GrADS software).

Supplementary Fig. 3 illustrates the presence of the shallow branch of the BDC in the model simulations. Additionally, the EP fluxes observed at the Arctic in the model simulations underscore the BDC's role in transporting aerosols from South and East Asia to the Arctic region. This transport is seen in anomalies of BC, OC, and sulfate aerosols (Fig. 2a–f). It should be noted that transport of aerosols emitted from East and South Asia to the Arctic and Southern hemisphere at  $\sim 40^{\circ}$  S occurs through the UTLS. Figure 2a–f shows that the average concentrations of East Asian BC ( $2.0 \text{ ng m}^{-3}$ ), OC ( $3 \text{ ng m}^{-3}$ ), and sulfate ( $52 \text{ ng m}^{-3}$ ) aerosols transported to the Arctic is larger than from South Asia (BC:  $1.1 \text{ ng m}^{-3}$ , OC:  $6 \text{ ng m}^{-3}$  and sulfate:  $40 \text{ ng m}^{-3}$ ). Negative anomalies (CTL-SASO or CTL-EASO) in Fig. 2 indicate that aerosols are not transported to those regions. The aerosol enhancement in the southern hemisphere-lower troposphere is due to downward transport from the UTLS and transport at lower levels.

The percentage change in amounts of aerosols (BC, OC, and sulfate) in the Arctic due to emission changes in South Asia and East Asia are larger in the UTLS than the troposphere, except for sulfate aerosols from South Asia (see Table 1). Thus, from Table 1 we see that the majority of aerosols from South and East Asia are transported to the Arctic via the UTLS. In the Arctic UTLS, there are larger amounts of East Asian aerosols (BC and sulfate) than in South Asia. While in the troposphere, South Asian aerosols are higher than in East Asia.

### Impact on Radiative Forcing in the Arctic during the monsoon season

Anthropogenic aerosols in the atmosphere scatter and absorb solar radiation, therefore leading to a reduction in surface solar radiation (i.e. a cooling effect) and, depending on the optical particle properties, to atmospheric warming or cooling. The aerosol loading and its associated RFari vary with time. Observations at the Arctic during 2005–2010 indicate a radiative forcing of  $-0.19 \pm 0.05 \text{ W m}^{-2}$  at the TOA due to the anthropogenic aerosol<sup>14</sup> and  $-0.24 \pm 0.1 \text{ W m}^{-2}$  during 1990–2010<sup>48</sup>. This suggests that Arctic aerosols have become relatively more absorbing in recent years.

We estimate the changes in net RFari over the Arctic due to all aerosols in the atmosphere, induced by emission changes over South Asia and East Asia (Fig. 3). Our simulations show that the aerosol radiative forcing in the Arctic due to aerosol transported from South Asia is  $-0.07 \pm 0.02 \text{ W m}^{-2}$  at

the surface and  $+0.004 \pm 0.001 \text{ W m}^{-2}$  at TOA (with a corresponding atmospheric forcing of  $+0.074 \pm 0.03 \text{ W m}^{-2}$ ). Similarly, the aerosol transported over the Arctic from East Asia also induces a RFari of  $-0.09 \pm 0.02 \text{ W m}^{-2}$  at the surface,  $-0.007 \pm 0.001 \text{ W m}^{-2}$  at the TOA (i.e., atmospheric RFari of  $+0.083 \pm 0.03 \text{ W m}^{-2}$ ).

The seasonal mean anthropogenic Asian aerosol radiative forcing at surface over the Arctic is characterized by a negative net forcing of  $-0.07 \pm 0.02 \text{ W m}^{-2}$  for South Asian and  $-0.09 \pm 0.02 \text{ W m}^{-2}$  for East Asian aerosol. This is primarily caused by the aerosol-related reduction in surface solar irradiation (dimming) during polar day. The net TOA forcing is positive for South Asian aerosols ( $+0.004 \pm 0.001 \text{ W m}^{-2}$ ) and negative for East Asian aerosols ( $-0.007 \pm 0.001 \text{ W m}^{-2}$ ). Therefore, the South Asian aerosol has a warming while East Asian aerosol has an overall cooling radiative influence on the Arctic climate. For the atmosphere, however, there are very different patterns of cooling and warming in the vertical depending on the air mass, as shown below in Fig. 4. While the net atmospheric forcing is relatively similar with values of  $+0.074 \text{ W m}^{-2}$  and  $+0.087 \text{ W m}^{-2}$  over the atmospheric column, the BC dominated aerosol from South Asia (see also Table 1 and Fig. 1) generally shows positive warming rates in the lower and middle troposphere as well as in the UTLS (Fig. 4a, c, e). This leads to a relatively minor cooling at the Earth's surface of only  $-0.043 \text{ K}$  and thus does not have a strongly deviating effect compared to the control case, at least near the surface. In contrast, the aerosol plumes from East Asia, which are dominated by sulfate aerosol and carry a larger amount of aerosol overall (see Table 1 and Fig. 1), are characterized by strong cooling in the troposphere due to shading and reflection of solar radiation as well as moderate warming in the UTLS (Fig. 4b, d, f). Accordingly, the reduction in the Arctic surface temperature is strong at  $-0.56 \text{ K}$  on an seasonal average.

### Impacts on heating rates

In this section, we show the impact of South and East Asian aerosols on the atmospheric heating rates, including their short-wave and long-wave components. The distribution of zonal mean heating rates (Fig. 4) shows the enhancement in heating along the transport pathways of aerosol into the UTLS and further to the Arctic due to the absorption of shortwave solar radiation (see Fig. 2a–f). The heating rates are significant at 95% confidence interval.

Figure 4a, b shows that South Asian emission enhances net heating rates by  $0.24 \text{ K yr}^{-1}$  to  $+0.86 \text{ K yr}^{-1}$  at the Arctic while East Asian emission cause a smaller change in heating rates of  $0$  to  $0.14 \text{ K yr}^{-1}$  at the Arctic UTLS (320–440 K). Figure 4a-f shows that the aerosol induced change in short wave heating rates is the dominating factor, with long wave heating negative changes in the Arctic UTLS (South Asia:  $-0.072 \text{ K yr}^{-1}$ , East Asia:  $-0.144 \text{ K yr}^{-1}$ ). The monsoon anticyclone region shows an enhancement in shortwave (SW) and longwave (LW) heating rates for South Asia emission (SW:  $2.16 \text{ K yr}^{-1}$ , LW:  $0.036 \text{ K yr}^{-1}$ ) and East Asia (SW:  $0.86 \text{ K yr}^{-1}$ , LW:  $0.072 \text{ K yr}^{-1}$ ); the larger heating rate changes in the ASMA region compared to the Arctic are due to the larger amounts of aerosol and gases (including water vapor).

The water vapor transport by the monsoon convection into the ASMA is further enhanced by the heating induced by the aerosol changes. It should be noted from Fig. 4 that South Asian aerosols produce higher heating in the Arctic UTLS (340–420 K) in comparison to East Asian aerosols although a larger amount of BC and sulfate aerosols are transported from East Asia to the Arctic (Table 1). The absorption of solar radiation by aerosols shifts where heating/warming occurs in the atmosphere, while simultaneously cooling the Earth’s surface through reduced surface solar radiation<sup>52</sup>.

We have further investigated the reason for less heating in the Arctic stratosphere due to East Asian aerosols. Our model simulations reveal a notable increase in the transport of water vapor into the Arctic, resulting in the cooling of the Arctic stratosphere (420–500 K). This phenomenon is more pronounced with East Asian aerosol emissions ( $\sim 0.16 \text{ ppmv}$ ) compared to South Asian emissions ( $\sim 0.025 \text{ ppmv}$ ), as illustrated in Fig. 5. Aerosol-induced atmospheric heating across the Asian region triggers temperature rises, consequently increasing evaporation rates. This

temperature enhancement is more significant for East Asian aerosols compared to South Asian aerosols (by approximately  $0.1 \text{ }^\circ\text{C}$ , see Fig. 5). The elevated temperature near the tropopause resulting from East Asian aerosols, in contrast to South Asian aerosols (by approximately  $0.18 \text{ }^\circ\text{C}$ ), facilitates increased water vapor entry into the stratosphere, consequently enhancing water vapor transport to the Arctic. This combined effect, where water vapor induces long-wave cooling while aerosols cause short-wave heating, contributes to the relatively diminished heating observed in the Arctic due to East Asian aerosols.

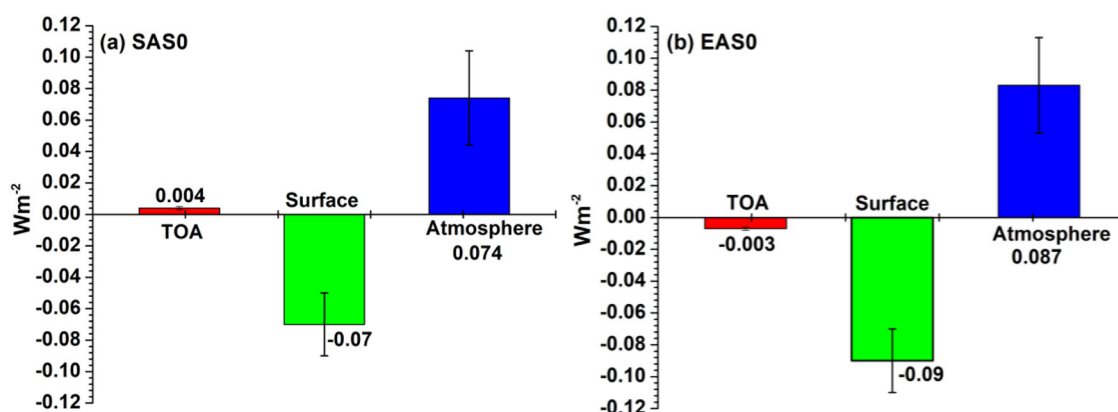
Furthermore, we show the vertical distribution of aerosol extinction (AE) and the heating rate anomalies over the Arctic ( $65^\circ\text{--}90^\circ\text{N}$ ) in Fig. 6a, b. The South Asian aerosols produce a maximum heating of  $0.14 \text{ K yr}^{-1}$  and an extinction ( $1.05\text{E-}4 \text{ km}^{-1}$ ) at the 380 K potential temperature level. Compared to the South Asian aerosols, the East Asian aerosols produce lower heating rates of  $0.11 \text{ K yr}^{-1}$  and extinction a maximum ( $0.38\text{E-}4 \text{ km}^{-1}$ ) at a lower level ( $\sim 360 \text{ K}$  level). The levels having higher amounts of absorbing aerosols (BC) are associated with higher heating rates. An average heating in the Arctic caused by East Asian aerosols  $\sim 0.11 \text{ K yr}^{-1}$  for all layers is much smaller than that caused by South Asian aerosols ( $0.14 \text{ K yr}^{-1}$ ).

Figure 7 illustrates the schematic representation of the effects of transporting anthropogenic Asian aerosols from South and East Asia to the Arctic via BDC through the monsoon anticyclone, along with their resulting impacts.

It must be noted that the prescribed anthropogenic emissions in the model affect the atmospheric burden, vertical layering and deposition of aerosol that will further impact on the atmospheric radiative balance and therefore the Arctic climate. In this paper, the aerosol transport from South and East Asia and radiative impacts at the Arctic are estimated based on the ECHAM6-HAMMOZ model simulations. There are uncertainties in the estimates of sea salt emission and its parameterization in the ECHAM6-HAMMOZ model<sup>53,54</sup> and the model also underestimates dust aerosols<sup>53</sup>. Also, ammonium nitrate aerosols are not included in the model. Recent in-situ measurements have shown ammonium nitrate aerosols as a major component in the monsoon anticyclone. The absence of ammonium nitrate aerosols in the model simulation may cause uncertainty to our results. However, such uncertainty will be minimal since they are absent in both control (CTL) and sensitivity simulations (SAS0, EAS0). Their impacts are subdued in anomalies (CTL-SAS0 or CTL-EAS0). It should be noted that sensitivity simulations are performed only for anthropogenic aerosols. Ammonium nitrate’s has major sources other than anthropogenic, that is large quantities from natural sources for example agriculture excreta from animals<sup>54</sup>. Since these uncertainties are the same in the CTL and sensitivity simulations SAS0 and EAS0, their relative influence on the anomalies investigated is less pronounced (i.e. CTL-SAS0 and CTL-EAS0).

**Table 1 | Percentage change in amounts of BC, OC, and sulfate aerosols at the Arctic (0–360 E, 65°–90° N) due emission changes in South Asia and East Asia in comparison to control at atmospheric layers (1) troposphere (280K–320K potential temperature levels) and (2) UTLS (320K–500K potential temperature levels)**

Species (experiment)	Troposphere (280–320 K)	UTLS (320–500 K)
OC (CTL-SAS0)	9.2%	11.2%
OC (CTL-EAS0)	4.6%	4.8%
BC (CTL-SAS0)	6.4%	15.8%
BC (CTL-EAS0)	4.8%	19.7%
Sulfate (CTL-SAS0)	3.8%	2%
Sulfate (CTL-EAS0)	0.8%	19.3%



**Fig. 3 | Changes in seasonal mean net Radiative Forcing at the Arctic due to aerosol transport from South Asia and East Asia. ECHAM6-HAMMOZ model estimated anomalies of seasonal mean net Radiative Forcing (RFari) ( $\text{W m}^{-2}$ ) at the**

**TOA and Surface and in the atmosphere over the Arctic due to aerosol transport from a South Asia (CTL-SAS0) and b East Asia (CTL-EAS0). (Figure created using the Origin, OriginLab, Northampton, MA).**

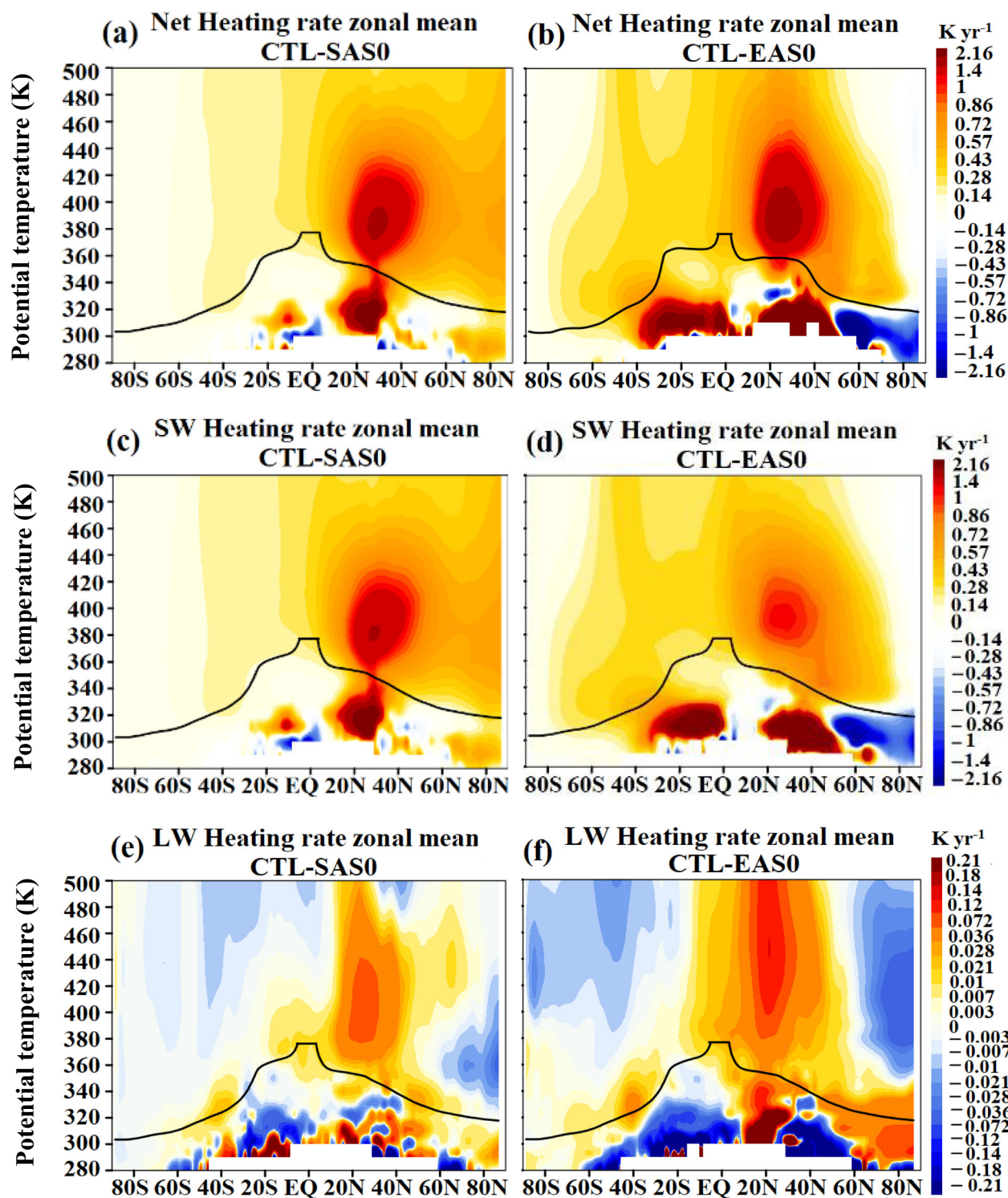


**Fig. 4 | Vertical variation of seasonal mean heating rates caused by aerosols from South Asia and East Asia.** Vertical distribution of seasonal and zonal mean heating rates  $\text{K yr}^{-1}$  for SAS0 and EAS0 emission simulations **a, b** net heating rates, **c, d** same as **(a, b)** but for short wave heating rates, **e, f** same as **(a, b)** but for long wave heating

rates. Color scale for figures for long wave heating rates is different than net and short wave heating rates. The black line of 2PV in **(a–f)** indicates the dynamical tropopause. (Figure created using the COLA/GrADS software).

Further, to have confidence in the simulated aerosol distribution in the UTLS, it is important to evaluate the ECHAM6-HAMMOZ (CTL) model performance against observations. In the past we have validated the simulated scattering ratio with CALIPSO and MIPAS satellite retrievals<sup>55</sup>. Our model shows reasonable agreement with CALIPSO and MIPAS satellite

retrievals of scattering ratio. The ECHAM-HAM model was recently evaluated specifically for the Arctic region against surface and airborne measurements<sup>56</sup>, particularly with respect to different emission source regions as well as globally with respect to the aerosol layering (including the Arctic) by<sup>57</sup> and<sup>58</sup>. The vertical distribution of BC aerosols shows general

**Fig. 5 | Vertical distribution of water vapor in response to aerosol emission changes over South Asia and East Asia.** Vertical distribution of zonal mean water vapor (ppm) for **a** South Asian emission simulations, **b** East Asian emission simulations. The black line of 2PV in (a, b) indicates the dynamical tropopause. Contours in cyan color are temperature anomalies ( $^{\circ}\text{C}$ ) (Figure created using the COLA/GrADS software).

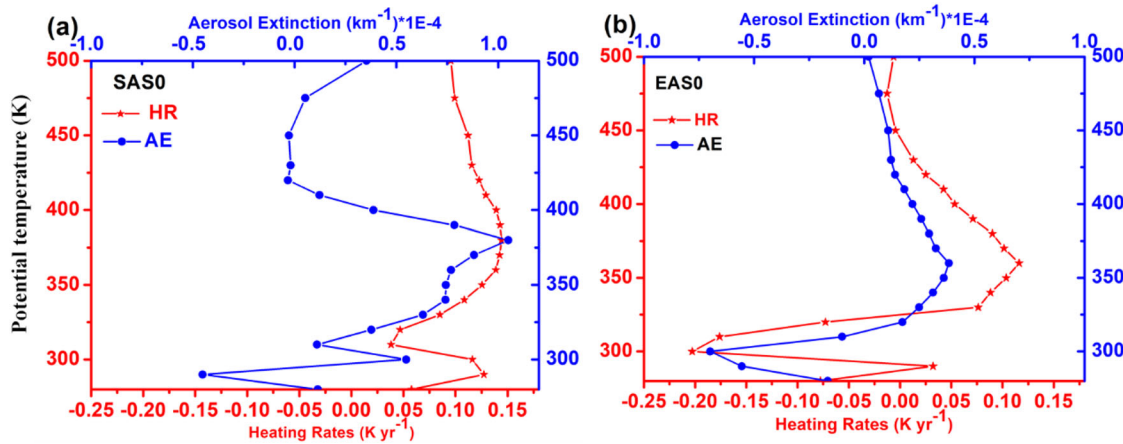
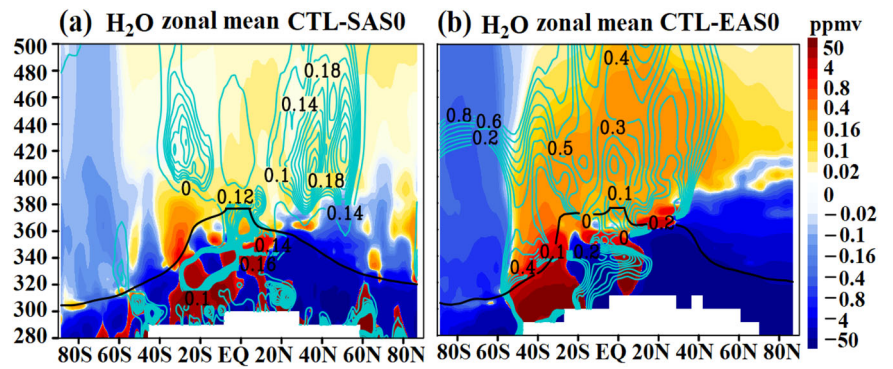


**Fig. 6 | Vertical profile of changes in aerosol extinction and the heating rate over the Arctic region.** Vertical profile of aerosol extinction ( $\text{km}^{-1}$ ) anomalies and the heating rate ( $\text{K yr}^{-1}$ ) over the Arctic region ( $65^{\circ}$ – $85^{\circ}\text{N}$ ) derived from a zonal average

of South Asian emission simulations, **b** zonal average of East Asian emission simulations. (Figure created using the Origin, OriginLab, Northampton, MA).

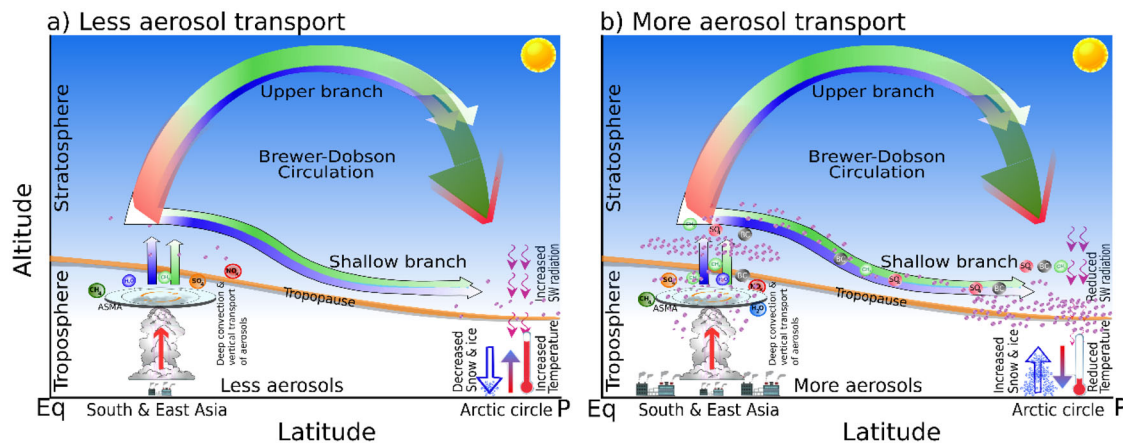


**Fig. 7 | A schematic depicting monsoon convection transporting aerosols to the Asian summer monsoon anticyclone and then to the Arctic.** A schematic depicting monsoon convection transporting aerosols to the Asian summer monsoon anticyclone (ASMA) and to the Arctic by lower branch of brewer dobson circulation

for model simulations with **a** anthropogenic aerosols over South/East Asia switched off (SASO or EASO), less aerosol scenario and **b** anthropogenic aerosols over South/East Asia (CTL) relatively more aerosol scenario. (Figure created using the Adobe illustrator).

agreement with observations, there is good agreement near the surface (correlation  $> 0.6$ ) while there is overestimation in the upper troposphere<sup>56</sup>. Some studies show that the ECHAM-HAMMOZ model underestimates accumulation-mode particles in the upper troposphere<sup>57</sup>.

It is difficult to differentiate the composition of the aerosol from satellite observations due to the small amounts of soot and sulfate in the

UTLS<sup>59</sup>. Hence, we evaluate simulated distribution of aerosols in the UTLS against different reanalysis data sets: (1) The Modern-Era Retrospective analysis for Research and Applications, Version 2 (MERRA-2), and (2) Copernicus Atmosphere Monitoring Service (CAMS) in methods (Section “The ECHAM6-HAMMOZ model simulations”). The model evaluation shows that the large-scale patterns in the aerosol distribution (e.g. BC and

OC maxima in the monsoon anticyclone), sulfate maximum in the extra-tropics (Supplementary Fig. 4a–i) is very similar for the model and reanalysis datasets with some disparities in the details of the aerosol distributions. In the following, the detailed differences are discussed further.

In the anticyclone region (Supplementary Fig. 4j) the BC loading is highest in MERRA-2 (MERRA-2: 85.2 kg/kg; ECHAM6-HAMMOZ: 23.9 kg/kg; CAMS: 19.6 kg/kg), the OC loading is highest in CAMS (CAMS: 364.9 kg/kg, MERRA-2: 213.2 kg/kg, ECHAM6-HAMMOZ: 57.5), while the sulfate aerosol loading is highest in ECHAM6-HAMMOZ (ECHAM6-HAMMOZ: 921.8 kg/kg; MERRA-2: 504.9 kg/kg; CAMS: 103.1 kg/kg).

The Arctic regions (Supplementary Fig. 4k) also show high amounts of BC in MERRA-2 (MERRA-2: 49.6 kg/kg, CAMS: 20.4 kg/kg; ECHAM6-HAMMOZ: 9.3 kg/kg), OC in CAMS (CAMS: 289.2 kg/kg; MERRA-2: 276.1 kg/kg; ECHAM6-HAMMOZ: 37.4 kg/kg) and sulfate in ECHAM6-HAMMOZ (ECHAM6-HAMMOZ: 1558.6 kg/kg; MERRA-2: 515.8 kg/kg; CAMS: 121.3 kg/kg). There are larger differences between the model and the reanalysis products among the species. Differences exist between the model and the reanalysis products across various species, attributed to variations in emission inventories, model transport processes, and assimilated products<sup>60</sup>. Generally, black carbon (BC) and organic carbon (OC) quantities are lower in ECHAM6-HAMMOZ compared to MERRA-2 and CAMS, while sulfate aerosols exhibit higher levels in ECHAM6-HAMMOZ than in MERRA-2 and CAMS.

Further, in Supplementary Fig. 5 we show the spread in data within the 16 ensemble members used in analysis (time average from 2001 to 2016) for Aerosol Optical depth (AOD), RF at the surface ( $Wm^{-2}$ ), and RF at the top of the atmosphere (TOA) ( $Wm^{-2}$ ) over South Asia, East Asia, and the Arctic regions. The 25th, 75th percentile and the median indicates moderate variability within 16 ensemble members in simulated anomalies of AOD and RF.

## Discussion

In this paper, we report the impact of the transport of South Asian and East Asian anthropogenic aerosols to the Arctic atmosphere during the monsoon season using ECHAM6-HAMMOZ simulations. The model simulations show that the deep monsoon convection transports South Asian and East Asian aerosols to the ASMA. The outflow of South Asian aerosol occurs at higher levels (360–380 K) than East Asian aerosols (330–350 K) indicating the role of the elevated orography of Himalayas. These aerosols then enter into the shallow branch of the BDC and are transported to the Arctic. The average concentrations of East Asian BC ( $2.0 ng m^{-3}$ ), OC ( $3 ng m^{-3}$ ), and sulfate ( $52 ng m^{-3}$ ) aerosols transported to the Arctic is larger than from South Asia (BC:  $1.1 ng m^{-3}$ , OC:  $6 ng m^{-3}$  and sulfate:  $40 ng m^{-3}$ ). The short-wave heating rate changes caused by East Asian aerosols ( $\sim 0.11 K yr^{-1}$ ) are lower than for South Asian aerosols ( $\sim 0.14 K yr^{-1}$ ) due to the different aerosol composition and the stronger water vapor transport (and associated long-wave cooling) to the Arctic stratosphere (420–500 K) caused by East Asian compared to South Asian aerosols. The vertical distribution of extinction and the heating rates anomalies over the Arctic show that South Asian aerosols produce maxima in extinction and heating at 380 K level (extinction:  $1.05E-4 km^{-1}$ , heating rate:  $0.14 K yr^{-1}$ ), compared to East Asian aerosols at 360 K (extinction:  $0.38E-4 km^{-1}$ , heating rates:  $0.11 K yr^{-1}$ ).

Radiative forcing estimates for the Arctic show that East Asian aerosols produce RF-ARI at the surface of  $-0.09 \pm 0.02 W m^{-2}$  and at the TOA of  $-0.003 \pm 0.001 W m^{-2}$ . For South Asian aerosols, the surface value is slightly lower with  $-0.07 \pm 0.02 W m^{-2}$  but the TOA forcing is actually positive with  $+0.004 \pm 0.001 W m^{-2}$ . This leads to a larger impact of East Asian aerosols on the Arctic surface temperature ( $-0.56 K$ ) than South Asian aerosols ( $-0.043 K$ ). For the South Asian aerosols transported to the Arctic region, the percentage change in amounts of the absorbing BC aerosol is larger than the scattering aerosols sulfate and OC. The warming caused by South Asian BC (positive anomalies at the TOA) counteract the cooling due to the scattering aerosols, leading to an overall small reduction in Arctic surface temperature ( $-0.043 K$ ). The large amounts of East Asian sulfate aerosols

reaching the Arctic contribute to a substantial surface cooling of  $-0.56 K$  in that region.

Thus, East Asian aerosols play an important role in offsetting the rapid Arctic surface temperature increase. However, it's important to note that the results presented here are derived from simulations using a single model, which may introduce uncertainties, particularly in terms of transport processes and the representation of aerosols and chemistry (Section "The ECHAM6-HAMMOZ model simulations"). Nevertheless, our findings provide insights into the radiative impact of long-range aerosol transport from Asia to the Arctic via BDC through the convection associated with the Asian summer monsoon.

## Methods

### The Modern-Era Retrospective analysis for Research and Applications, Version 2 (MERRA-2)

The Modern-Era Retrospective analysis for Research and Applications, Version 2 (MERRA-2) provides data from 1980. MERRA-2 replaces the original MERRA dataset. It includes advances in both the GEOS model and the GSI assimilation system. It also contains interactive analysis of aerosols that feed back into the circulation along with the meteorological data using a modern satellite database (GMAO, 2015). AERONET (1999–October 2014), Multi-angle Imaging Spectro Radiometer (MISR, February 2000–June 2014), MODIS Terra (March 2000 onwards), and MODIS Aqua (August 2002 onwards). MISR aerosol information is assimilated over the bright land surface<sup>61</sup>. We analysed seasonal mean (June to September) obtained from 3 hourly MERRA-2 mixing ratio of BC (Hydrophilic black carbon and Hydrophobic black carbon), OC (Hydrophilic organic matter and Hydrophobic organic matter), and Sulfate aerosols, during 2001–2016 at  $0.5^\circ \times 0.625^\circ$  latitude  $\times$  longitude grid.

### The Copernicus Atmosphere Monitoring Service (CAMS)

The CAMS reanalysis uses 4DVar data assimilation in Cycle 42r1 of ECMWF's Integrated Forecasting System (IFS), with 60 hybrid sigma/pressure (model) levels in the vertical, with the top level at 0.1 hPa. The aerosol module of IFS is a bulk-bin scheme simulating five types of aerosols with 12 prognostic tracers. There are three organic matter, and black carbon with the hydrophilic and hydrophobic component, and sulfate aerosol. CAMS reanalysis assimilated satellite data of the Envisat Advanced Along-Track Scanning Radiometer (AATSR), MODIS/Terra, and MODIS/Aqua<sup>61,62</sup>. We analysed seasonal mean obtained from 3 h, mixing ratio of BC (Hydrophilic black carbon and Hydrophobic black carbon), OC (Hydrophilic organic matter and Hydrophobic organic matter), and Sulfate aerosols, during 2003–2016 at the  $0.75^\circ \times 0.75^\circ$  latitude  $\times$  longitude grid.

### The ECHAM6-HAMMOZ model simulations

We use the state-of-the-art ECHAM6-HAMMOZ aerosol-chemistry-climate model to understand the transport pathways of South and East Asian aerosols to the Arctic. The model comprises the general circulation module ECHAM6, coupled with the aerosol module HAM<sup>60,63</sup>. HAM predicts the formation and sink of sulfate, BC, particulate organic matter (POM), sea salt (SS), and mineral dust (DU) aerosols. HAM explicitly simulates the aerosol species' effects on cloud droplets and ice crystal formation, as the aerosol particles act as cloud condensation nuclei or ice-nucleating particles. In the model there is feedback of the aerosol change to the radiation and the atmospheric circulation. The emission inventory for anthropogenic aerosol and the sulfate, black carbon (BC), and organic carbon (OC) from fire emission was taken based on the Coupled Model Inter-comparison Project phase 6 (CMIP6). Details of the model and emissions are given by past studies<sup>64–66</sup>.

The model was employed at the T63 spectral resolution corresponding to  $1.875 \times 1.875$  degrees in the horizontal dimension and at 47 hybrid  $\sigma$ -p levels in the vertical from the surface up to 0.01 hPa, with 7.5 min time step length. The monthly average data from Atmospheric Model Inter-comparison Project (AMIP) sea surface temperature (SST) and sea ice cover (SIC)<sup>67</sup> were used as lower boundary conditions. We performed three



experiments: (1) control simulations (CTL) where all aerosols are present and two sensitivity experiments where anthropogenic aerosols are switched off over (2) South Asia referred to as SASO (68°–95° E, 8–38° N) and (3) East Asia referred to as EASO (78°E–145°E, 20°N–50°N). All simulations were performed for the period 1 January 2001 to 31 December 2016, from stabilized initial fields, created after the model integration of one year. The analysis is performed for the monsoon season (June–September) from 2001–2016. The difference between CTL and SASO simulations gives information on South Asian anthropogenic aerosols; similarly, information on East Asian anthropogenic aerosols is obtained from the difference between CTL and EASO simulations.

### Data availability

Available from the corresponding author upon reasonable request.

### Code availability

Available from the corresponding author upon reasonable request.

Received: 28 July 2023; Accepted: 31 March 2024;

Published online: 13 May 2024

### References

- IPCC, 2007: Climate Change 2007: The Physical Science Basis. Contribution of Working Group I to the Fourth Assessment Report of the Intergovernmental Panel on Climate Change [Solomon, S., et al. and, 996 pp. Fourth assessment report of the Intergovernmental Panel on Climate Change: Important observations and conclusions. *Curr. Sci.* **92**, 1034 (2007).
- Stocker, T. F. et al. Climate Change 2013 The Physical Science Basis: Working Group I contribution to the fifth assessment report of the intergovernmental panel on climate change. *Clim. Chang.* **9781107057**, 1–1535 (2013).
- Intergovernmental Panel on Climate Change. *Climate Chang.* <https://doi.org/10.1017/9781009157896> (2023).
- Yu, L., Leng, G. & Tang, Q. Varying contributions of greenhouse gases, aerosols and natural forcings to Arctic land surface air temperature changes. *Environ. Res. Lett.* **17**, 124004 (2022).
- Rantanen, M. et al. The Arctic has warmed nearly four times faster than the globe since 1979. *Commun. Earth Environ.* **3**, 1–10 (2022).
- Pithan, F. & Jung, T. Arctic amplification of precipitation changes—the energy hypothesis. *Geophys. Res. Lett.* **48**, 1–9 (2021).
- Bond, T. C. et al. Bounding the role of black carbon in the climate system: a scientific assessment. *J. Geophys. Res. Atmos.* **118**, 5380–5552 (2013).
- Myhre, G. et al. Anthropogenic and natural radiative forcing. *Clim. Chang.* **123**, 2176–2218 (2013).
- Yasunari, T. J., Koster, R. D., Lau, W. K. M. & Kim, K.-M. Impact of snow darkening via dust, black carbon, and organic carbon on boreal spring climate in the Earth system. *J. Geophys. Res. Atmos.* **120**, 5485–5503 (2015).
- Fadnavis, S. et al. Air pollution reductions caused by the COVID-19 lockdown open up a way to preserve the Himalayan glaciers. *Atmos. Chem. Phys.* **23**, 10439–10449 (2023).
- Flanner, M. G. et al. Springtime warming and reduced snow cover from carbonaceous particles. *Atmos. Chem. Phys.* **9**, 2481–2497 (2009).
- Notz, D. & Community, S. Arctic Sea Ice in CMIP6. *Geophys. Res. Lett.* **47**, e2019GL086749 (2020).
- Ren, L. et al. Source attribution of Arctic black carbon and sulfate aerosols and associated Arctic surface warming during 1980–2018. *Atmos. Chem. Phys.* **20**, 9067–9085 (2020).
- Yang, Y., Wang, H., Smith, S. J., Easter, R. C. & Rasch, P. J. Sulfate aerosol in the Arctic: source attribution and radiative forcing. *J. Geophys. Res. Atmos.* **123**, 1899–1918 (2018).
- Charlson, R. J. et al. Climate forcing by anthropogenic aerosols. *Science* **255**, 423–430 (1992).
- Lou, S. et al. Black carbon increases frequency of extreme ENSO events. *J. Clim.* **32**, 8323–8333 (2019).
- AMAP: AMAP Assessment 2015: Black carbon and ozone as Arctic climate forcers, Arctic Monitoring and Assessment Programme (AMAP), Oslo, Norway. *Arct. Monit. Assess. Progr.* **33**, 1–12 (2015).
- Breider, T. J. et al. Multidecadal trends in aerosol radiative forcing over the Arctic: contribution of changes in anthropogenic aerosol to Arctic warming since 1980. *J. Geophys. Res.* **122**, 3573–3594 (2017).
- Sand, M., Samset, B. H., Tsigaridis, K., Bauer, S. E. & Myhre, G. Black carbon and precipitation: an energetics perspective. *J. Geophys. Res. Atmos.* **125**, (2020).
- Shindell, D. T. et al. A multi-model assessment of pollution transport to the Arctic. *Atmos. Chem. Phys.* **8**, 5353–5372 (2008).
- Fadnavis, S. et al. Elevated aerosol layer over South Asia worsens the Indian droughts. *Sci. Rep.* **9**, 1–11 (2019).
- Di Pierro, M., Jaeglé, L. & Anderson, T. L. Satellite observations of aerosol transport from East Asia to the Arctic: three case studies. *Atmos. Chem. Phys.* **11**, 2225–2243 (2011).
- Matsui, H. et al. Accumulation-mode aerosol number concentrations in the Arctic during the ARCTAS aircraft campaign: Long-range transport of polluted and clean air from the Asian continent. *J. Geophys. Res. Atmos.* **116**, 1–14 (2011).
- Ikeda, K. et al. Model and satellite analysis of transport of Asian anthropogenic pollution to the Arctic: Siberian and Pacific pathways and their meteorological controls. *J. Geophys. Res. Atmos.* **126**, 1–15 (2021).
- Huang, Z. et al. Short-cut transport path for Asian dust directly to the Arctic: a case study. *Environ. Res. Lett.* **10**, 114018 (2015).
- Backman, J., Schmeisser, L. & Asmi, E. Asian emissions explain much of the Arctic black carbon events. *Geophys. Res. Lett.* **48**, (2021).
- Ikeda, K. et al. Tagged tracer simulations of black carbon in the Arctic: transport, source contributions, and budget. *Atmos. Chem. Phys.* **17**, 10515–10533 (2017).
- Sharma, S. et al. 16-year simulation of Arctic black carbon: transport, source contribution, and sensitivity analysis on deposition. *J. Geophys. Res. Atmos.* **118**, 943–964 (2013).
- Fadnavis, S. et al. Transport of aerosols into the UTLS and their impact on the Asian monsoon region as seen in a global model simulation. *Atmos. Chem. Phys.* **13**, 8771–8786 (2013).
- Fadnavis, S., Kalita, G., Ravi Kumar, K., Gasparini, B. & Li, J. L. F. Potential impact of carbonaceous aerosol on the upper troposphere and lower stratosphere (UTLS) and precipitation during Asian summer monsoon in a global model simulation. *Atmos. Chem. Phys.* **17**, 11637–11654 (2017).
- Fadnavis, S., Roy, C., Sabin, T. P., Ayantika, D. C. & Ashok, K. Potential modulations of pre-monsoon aerosols during El Niño: impact on Indian summer monsoon. *Clim. Dyn.* **49**, 2279–2290 (2017).
- Randel, W. J. et al. Asian monsoon transport of pollution to the stratosphere. *Science* **328**, 611–613 (2010).
- Randel, W. J. & Park, M. Deep convective influence on the Asian summer monsoon anticyclone and associated tracer variability observed with Atmospheric Infrared Sounder (AIRS). *J. Geophys. Res. Atmos.* **111**, 1–13 (2006).
- Brunamonti, S. et al. Balloon-borne measurements of temperature, water vapor, ozone and aerosol backscatter on the southern slopes of the Himalayas during StratoClim 2016–2017. *Atmos. Chem. Phys.* **18**, 15937–15957 (2018).
- Hanumanthu, S. et al. Strong day-to-day variability of the Asian Tropopause Aerosol Layer (ATAL) in August 2016 at the Himalayan foothills. *Atmos. Chem. Phys.* **20**, 14273–14302 (2020).
- Vernier, J. P., Thomason, L. W. & Kar, J. CALIPSO detection of an Asian tropopause aerosol layer. *Geophys. Res. Lett.* **38**, 1–6 (2011).
- Vernier, H. et al. Exploring the inorganic composition of the Asian Tropopause Aerosol Layer using medium-duration balloon flights. *Atmos. Chem. Phys.* **22**, 12675–12694 (2022).

38. Höpfner, M. et al. Ammonium nitrate particles formed in upper troposphere from ground ammonia sources during Asian monsoons. *Nat. Geosci.* **12**, 608–612 (2019).
39. Appel, O. et al. Chemical analysis of the Asian tropopause aerosol layer (ATAL) with emphasis on secondary aerosol particles using aircraft-based in situ aerosol mass spectrometry. *Atmos. Chem. Phys.* **22**, 13607–13630 (2022).
40. Fadnavis, S. et al. Transport of trace gases via eddy shedding from the Asian summer monsoon anticyclone and associated impacts on ozone heating rates. *Atmos. Chem. Phys.* **18**, 11493–11506 (2018).
41. Zheng, C. et al. Summertime transport pathways from different northern hemisphere regions into the Arctic. *J. Geophys. Res. Atmos.* **126**, 1–23 (2021).
42. Park, M., Randel, W. J., Gettelman, A., Massie, S. T. & Jiang, J. H. Transport above the Asian summer monsoon anticyclone inferred from Aura Microwave Limb Sounder tracers. *J. Geophys. Res. Atmos.* **112**, 1–13 (2007).
43. Santee, M. L. et al. A comprehensive overview of the climatological composition of the Asian summermonsoon anticyclone based on 10 years of Aura Microwave Limb Sounder measurements. *J. Geophys. Res.* **122**, 5491–5514 (2017).
44. Vogel, B. et al. Reconstructing high-resolution in-situ vertical carbon dioxide profiles in the sparsely monitored Asian monsoon region. *Commun. Earth Environ.* **4**, (2023).
45. Ploeger, F. et al. Horizontal water vapor transport in the lower stratosphere from subtropics to high latitudes during boreal summer. *J. Geophys. Res. Atmos.* **118**, 8111–8127 (2013).
46. Yan, X., Konopka, P., Hauck, M., Aurelien, P. & Ploeger, F. Asymmetry and pathways of inter-hemispheric transport in the upper troposphere and lower stratosphere. *Atmos. Chem. Phys.* **21**, 6627–6645 (2021).
47. Gottschaldt, K. D. et al. Dynamics and composition of the Asian summer monsoon anticyclone. *Atmos. Chem. Phys.* **18**, 5655–5675 (2018).
48. Im, U. et al. Present and future aerosol impacts on Arctic climate change in the GISS-E2.1 Earth system model. *Atmos. Chem. Phys.* **21**, 10413–10438 (2021).
49. Fadnavis, S. et al. Trends in peroxyacetyl nitrate (PAN) in the upper troposphere and lower stratosphere over southern Asia during the summer monsoon season: Regional impacts. *Atmos. Chem. Phys.* **14**, 12725–12743 (2014).
50. Fadnavis, S. et al. Transport pathways of peroxyacetyl nitrate in the upper troposphere and lower stratosphere from different monsoon systems during the summer monsoon season. *Atmos. Chem. Phys.* **15**, 11477–11499 (2015).
51. Eichelberger, S. J. & Hartmann, D. L. Changes in the strength of the Brewer–Dobson circulation in a simple AGCM. *Geophys. Res. Lett.* **32**, 1–5 (2005).
52. Ramanathan, V., Crutzen, P. J., Kiehl, J. T. & Rosenfeld, D. Aerosols, climate, and the hydrological cycle. *Science* **294**, 2119–2124 (2001).
53. Kokkola, H. et al. SALSA2.0: The sectional aerosol module of the aerosol-chemistry-climate model ECHAM6.3.0-HAM2.3-MOZ1.0. *Geosci. Model Dev.* **11**, 3833–3863 (2018).
54. Bouwman, A. F. et al. A global high-resolution emission inventory for ammonia. *Glob. Biogeochem. Cycles* **11**, 561–587 (1997).
55. Fadnavis, S. et al. The role of tropical volcanic eruptions in exacerbating Indian droughts. *Sci. Rep.* **11**, 1–13 (2021).
56. Schacht, J. et al. The importance of the representation of air pollution emissions for the modeled distribution and radiative effects of black carbon in the Arctic. *Atmos. Chem. Phys.* **19**, 11159–11183 (2019).
57. Watson-Parris, D. et al. In situ constraints on the vertical distribution of global aerosol. *Atmos. Chem. Phys.* **19**, 11765–11790 (2019).
58. Kühn, T. et al. Effects of black carbon mitigation on Arctic climate. *Atmos. Chem. Phys.* **20**, 5527–5546 (2020).
59. Tackett, J. L. et al. The CALIPSO version 4.5 stratospheric aerosol subtyping algorithm. *Atmos. Meas. Tech.* **16**, 745–768 (2023).
60. Tegen, I. et al. The global aerosol-climate model echem6.3-ham2.3 -Part 1: Aerosol evaluation. *Geosci. Model Dev.* **12**, 1643–1677 (2019).
61. Zhang, T., Zang, L., Mao, F., Wan, Y. & Zhu, Y. Evaluation of Himawari-8/AHI, MERRA-2, and CAMS aerosol products over China. *Remote Sens.* **12**, 1–16 (2020).
62. Inness, A. et al. The CAMS reanalysis of atmospheric composition. *Atmos. Chem. Phys.* **19**, 3515–3556 (2019).
63. Stier, P. et al. The aerosol-climate model ECHAM5-HAM. *Atmos. Chem. Phys.* **5**, 1125–1156 (2005).
64. Fadnavis, S. et al. A rising trend of double tropopauses over South Asia in a warming environment: Implications for moistening of the lower stratosphere. *Int. J. Climatol.* **41**, E200–E215 (2021).
65. Fadnavis, S. & Chattopadhyay, R. Linkages of subtropical stratospheric intraseasonal intrusions with Indian summer monsoon deficit rainfall. *J. Clim.* **30**, 5083–5095 (2017).
66. Fadnavis, S. et al. The impact of recent changes in Asian anthropogenic emissions of SO<sub>2</sub> on sulfate loading in the upper troposphere and lower stratosphere and the associated radiative changes. *Atmos. Chem. Phys. Discuss.* 1–44 <https://doi.org/10.5194/acp-2019-81> (2019).
67. Taylor, K. E., Williamson, D. L. & Zwiers, F. W. The Sea Surface Temperature and Sea-Ice Concentration Boundary Conditions for AMIP II Simulations, Program for Climate Model Diagnosis and Intercomparison (PCMDI) Report 60. *Lawrence Livermore Natl. Lab. Livermore, Calif.* 1–28 (2000).

## Acknowledgements

The authors thank the staff of the High-Power Computing Centre (HPC) in the Indian Institute of Tropical Meteorology, Pune, India, Pune, India. The authors thank Jean-Paul Vernier, National Institute of Aerospace, Hampton, VA, USA, for providing information on limitation of detection of small amounts sulfate and soot in the UTLS region against larger amounts from volcanoes and wildfires. The authors are also thankful to Satheesh Chandran P. R., Indian Institute of Tropical Meteorology, India for valuable suggestions. Authors also thank Mian Chin, NASA Goddard Space Flight Center, USA for her valuable help. B.H. gratefully acknowledges funding by the Deutsche Forschungsgemeinschaft (DFG, German Research Foundation) – Projektnummer 268020496 – TRR 172, within the Transregional Collaborative Research Center “Arctic Amplification: Climate Relevant Atmospheric and Surface Processes, and Feedback Mechanisms (AC)3 in subproject D02.

## Author contributions

S. F. initiated the idea and performed analysis. S. S. helped analysis of model simulations. A. L. and S. F. designed model simulations. The information of transport processes and impacts at the Arctic is analysed and supported by B. H., F. P. A. R. T. S. and R.M. All authors contributed to the writing and discussions of the manuscript.

## Competing interests

The authors declare no competing interests.

## Additional information

**Supplementary information** The online version contains supplementary material available at <https://doi.org/10.1038/s41612-024-00633-1>.

**Correspondence** and requests for materials should be addressed to Suvama Fadnavis.

**Reprints and permissions information** is available at <http://www.nature.com/reprints>

**Publisher's note** Springer Nature remains neutral with regard to jurisdictional claims in published maps and institutional affiliations.

**Open Access** This article is licensed under a Creative Commons Attribution 4.0 International License, which permits use, sharing, adaptation, distribution and reproduction in any medium or format, as long as you give appropriate credit to the original author(s) and the source, provide a link to the Creative Commons licence, and indicate if changes were made. The images or other third party material in this article are included in the article's Creative Commons licence, unless indicated otherwise in a credit line to the material. If material is not included in the article's Creative Commons licence and your intended use is not permitted by statutory regulation or exceeds the permitted use, you will need to obtain permission directly from the copyright holder. To view a copy of this licence, visit <http://creativecommons.org/licenses/by/4.0/>.

© The Author(s) 2024